Receptor−Antagonist Interactions in the Complexes of Agouti and Agouti-Related Protein with Human Melanocortin 1 and 4 Receptors[†,‡]

Biao-Xin Chai,[*,§,||] Irina D. Pogozheva,[||,⊥] Yu-Mei Lai,[§] Ji-Yao Li,[§] Richard R. Neubig,[#] Henry I. Mosberg,[⊥] and Ira Gantz[§]

Departments of Surgery, Pharmacology and Internal Medicine, School of Medicine, and Department of Medicinal Chemistry, College of Pharmacy, University of Michigan, Ann Arbor, Michigan 48109

Received October 1, 2004; Revised Manuscript Received December 15, 2004

ABSTRACT: The molecular interactions between human melanocortin receptor-1 and -4 (hMC1R and hMC4R) and their endogenous antagonists, agouti signaling protein (ASIP) and agouti-related protein (AGRP), were assessed by studying the effects of site-directed mutations on the binding affinity of ^{125}I-ASIP[90−132(L89Y)] and ^{125}I-AGRP(86−132). Mutations of homologous residues from transmembrane helices (TMHs) 3 and 6 and extracellular loop (EL) 3 (D121A, T124A, F257A, and F277M in hMC1R and D126A, I129A F261A, and M281F in hMC4R) impaired binding of both antagonists to hMC4R and binding of the ASIP fragment to hMC1R. However, the mutations in TMH2 (E94A in hMC1R and E100A in hMC4R), TMH7 (F280A in hMC1R and F284A in hMC4R), and EL2 (Y183S, H184S, and D184H in hMC1R) only significantly affected binding of the ASIP fragment. The dependence of agonist binding on the dithiothreitol concentration followed a monophasic curve for wild-type hMC4R and its C40A, C271A, and C279A mutants and a biphasic curve for hMC1R, suggesting the presence of at least one structurally and functionally essential disulfide bond in both wild-type receptors and the hMC4R mutants. Models of complexes of both receptors with the ASIP fragment and hMC4R with the AGRP fragment were calculated using constraints from the experimental structures of rhodopsin and AGRP fragments, a set of deduced hydrogen bonds, supplemented by two proposed disulfide bridges and receptor−ligand contacts, derived from our mutagenesis data. In the models of the ASIP fragment complexed with both receptors, the core ligand tripeptide, Arg-Phe-Phe, positioned between TMHs 3 and 6, is shifted toward TMHs 2 and 7 relative to its position in the AGRP−hMC4R model, while the N-terminal loop and two central disulfides of the antagonists interact with EL2 of the receptors.

The melanocortin receptors (MCRs)[1] belong to the superfamily of seven transmembrane G-protein coupled receptors (GPCR). MCRs are positively coupled to cAMP generation by adenylate cyclase via the stimulatory G_s protein and are involved in other pathways (*1*, *2*), thus regulating a diverse number of physiological functions including pigmentation, steroidogenesis, energy homeostasis, exocrine secretion, sexual function, analgesia, inflammation, immunomodulation, temperature control, cardiovascular regulation, and neuromuscular regeneration (*1*).

The MCRs are unique among GPCRs with regard to the existence of endogenous antagonists, agouti/agouti signaling protein (ASIP) and agouti-related protein (AGRP) (*3*). Antagonists demonstrate subtype specificity for the five MCRs (*4*): agouti/ASIP has nanomolar affinity for MC1R, MC2R, and MC4R, a much lower affinity for MC3R, and no affinity for MC5R; AGRP has nanomolar affinity for MC3R and MC4R and very little affinity for MC1R, MC2R, and MC5R. Agouti has a central role in determining skin and coat color, acting as a competitive antagonist of α-melanocyte stimulating hormone (MSH) at the hair follicle MC1R. The role of ASIP in humans is unclear. AGRP participates in energy homeostasis in mammals and is an orexigenic factor by virtue of its ability to competitively antagonize MSH at the MC3R and MC4R (*5*, *6*).

Numerous studies have examined structural and functional aspects of AGRP and ASIP, which are composed of an N-terminal domain and a C-terminal cysteine-rich domain. It was shown that C-terminal AGRP fragments, AGRP(87−132) and AGRP(87−120) competitively antagonize MSH with equal potency as the full-length protein (*6*−*8*) and act as inverse agonists of a constitutively active MC4R (*9*−*13*).

[†] This work was supported by NIH Grants DK054032 (to I.G.), and DA03910 (to H.I.M.), HL46417 (to R.N.) and the University of Michigan Gastrointestinal Peptide Research Center (NIH Grant P30DK34933).

[‡] The described models of hMC1−ASIP(93-132), hMC4−ASIP(93-132), and hMC4−AGRP(87-132) are publicly available through http://mosberglab.phar.umich.edu/resources/.

* To whom correspondence should be addressed: Room 1524 MSRB I, 1150 W. Medical Center, Ann Arbor, MI 48109. Telephone: 734-763-0953. Fax: 734-763-2535. E-mail: bxchai@umich.edu.

[§] Department of Surgery, School of Medicine.

[||] Contributed equally to this work.

[⊥] Department of Medicinal Chemistry, College of Pharmacy.

[#] Pharmacology and Internal Medicine, School of Medicine.

[1] Abbreviations: AGRP, agouti-related protein; ASIP, agouti signaling protein (human homologue of agouti); GPCR, G-protein coupled receptor; MCR, melanocortin receptor; MSH, α-melanocyte stimulating hormone; NDP-MSH, [Nle^4,D-Phe^7]-α-melanocyte stimulating hormone; TMH, transmembrane helix; DTT, dithiothreitol.

10.1021/bi0478704 CCC: $30.25
Published on Web 02/08/2005

Pharmacological studies established that the conserved tripeptide Arg-Phe-Phe represents a key element required for agouti/ASIP and AGRP function (*14*−*16*). This differs from the agonist (adrenocorticotropic or MSH) pharmacophore, His-Phe-Arg-Trp (*17*).

Recently obtained NMR structures of the fragment AGRP-(87−132) (*18*) and AGRP(87−120) (*8*) revealed an inhibitor cystine knot motif that was previously found only in invertebrate neurotoxins (*19*). The structure of AGRP(87−132) consists of a β hairpin with an additional β strand and 3 loops and is stabilized by 5 conserved disulfide bonds. The structure of the smaller fragment AGRP(87−120), which lacks the C-terminal flexible loop, overlaps AGRP(87−132) at the three β strands but has a somewhat different conformation of the N-terminal loop. In both structures, the pharmacophoric element, Arg-Phe-Phe, is located at the apex of the β-hairpin turn region 111−113. While this triplet is essential to ligand−receptor interactions, it is not sufficient for selective high-affinity binding to MCRs and for full antagonist potency (*14*). Possibly, the residues from N-terminal loop 94−101 of AGRP or residues flanking the central β hairpin may represent the additional receptor-binding interface (*20*, *21*).

MCR−antagonist interactions have been studied by extensive site-directed mutagenesis and creation of receptor chimeras, which highlighted a set of residues forming the ligand-binding pockets for MSH and AGRP (*10*, *15*, *17*, *22*, *23*). It was found that only a few mutations in MC4R, such as E100K, D122R, D126A,N,K, D122A,N/D126A,N, F184K, Y187C, F201S, and F262S affected the binding and antagonist properties of AGRP (*17*, *23*). These data suggested that the Arg-Phe-Phe triplet of AGRP might interact with a cluster of negatively charged residues in transmembrane helix (TMH)3 and aromatic residues in TMHs 4, 5, and 6 of MC4R (*17*, *23*). Cassette substitutions in MC4R underlined the importance of TMH3 and TMH4 for binding of core octapeptide AGRP(110−117) (*15*), while the studies of chimeric receptor constructs revealed the essential role of EL2 and EL3 of MC4R in the binding of the larger fragment, AGRP(87−132) (*22*). The data obtained allowed the development of a model describing the interactions between AGRP with MC4R (*24*).

However, our understanding of molecular interactions between MCRs and their antagonists is incomplete. Notably, no data are available regarding hMC1R and hMC4R residues that are involved in agouti/ASIP binding. Moreover, the reason for the selectivity of AGRP to MC4R versus MC1R is incompletely understood. The studies herein were designed to compare the molecular interactions of hMC1R and hMC4R with their natural antagonists, ASIP and AGRP, respectively. To achieve this goal, we used a combination of receptor mutagenesis and molecular modeling. The models of receptor−antagonist complexes were calculated by the distance geometry algorithm using structural constraints derived from the rhodopsin X-ray structure (*25*, *26*), NMR structures of AGRP(87−132) (*18*) and AGRP(87−120) (*8*), predicted receptor-specific disulfide bridges, and a set of hydrogen bonds between receptor polar residues, together with receptor−ligand contacts derived from our current and previously published mutagenesis data.

EXPERIMENTAL PROCEDURES

Site-Directed Mutagenesis. The wild-type hMC1R and hMC4R and all mutants were expressed from the eukaryotic expression vector pcDNA3.1 (Invitrogen, Carlsbad, CA). For these studies, several new mutants were designed for hMC4R (C40A, I129A, F284A, S180F, F201A, F262A, F261A/F262A, L265A, M281F, F184A, S188Y, D189H, S190H, C271A, C277A, and C279A) and for hMC1R (T124A, W254A, L284A, M128A, F175S, F258A, L261A, I264Y, F277M, Y183S, D184H, H185S, E269Q, E269S, T272Y, D184H/E269S, and H185S/T272Y). The remainder of the mutations had been constructed during the course of previous studies (*17*, *27*). C277A, C279A, and F284A have been reported upon by others (*39*, *42*). New mutations were constructed using the QuickChange Site-Directed Mutagenesis Kit (Stratagene, La Jolla, CA). The presence of desired mutations and the integrity of the entire receptor sequence were confirmed by sequencing performed at the University of Michigan Biochemistry Core. Large-scale plasmid preparations were made using a Qiagen Plasmid Maxi Kit (Qiagen, Valencia, CA).

Cell Transfection and Culture. For these studies, HEK 293 cells in a 10 cm dish were transiently transfected with 5 μg of receptor plasmid DNA using 20 μL of Lipofectamine Reagent (Invitrogen, Carlsbad, CA). After 24 h, the cells were trypsinized and aliquoted into 24-well plates and grown in Dulbecco's modified Eagle medium (DMEM) containing 4.5 g/100 mL glucose, 10% fetal calf serum, and 1 mM sodium pyruvate.

Ligand Binding. ^{125}I-[Nle^4,D-Phe^7]-α-Melanocyte stimulating hormone (NDP-MSH), ^{125}I-AGRP(86−132), and ^{125}I-ASIP[90−132(L89Y)] were prepared by the chloramine-T method as previously described (*28*). NDP-MSH was purchased from Peninsula Laboratories, Inc. and AGRP(86−132), from Peptides International. Several batches of each radioligand were required for the binding experiments. The specific activity of radioligands were 618−727 Ci/mmol ^{125}I-NDP-MSH, 504−637 Ci/mmol ^{125}I-AGRP(86−132), and 665−790 Ci/mmol ^{125}I-ASIP[90−132(L89Y)]. Binding experiments were performed using 0.35 nM of radioligand. Binding assays were performed as previously described (*27*). A total of 3×10^5 cells were planted on 24-well plates and cultured for ∼17−19 h before the experiments. IC_{50} values were determined from the displacement of the radioligand by increasing concentrations of the same nonlabeled peptide. The highest nonlabeled peptide concentration used was 10^{-6} M. Nonspecific binding were determined in the presence of cold ligand at 10^{-5} M. Nonspecific binding was less than 7% of specific binding. IC_{50} values are reported as the mean ± standard error. To calculate K_i values using the same compound as the radioligand and competitor, the equation $K_i = K_d = IC_{50} -$ [radioligand] was used (*29*). To quantify receptor expression, competitive binding assays were performed to determine the amount of receptor protein according to the equation $B_{max} =$ [total binding − nonspecific binding]/[radioligand]/(K_d + [radioligand] (Graphpad Prism, Graphpad Software, San Diego, CA). Experiments were repeated at least 3 times using duplicate wells on different days.

3′,5′-Adenosine Monophosphate (cAMP) Measurement. cAMP measurements were performed using a competitive binding assay kit (TRK 432, Amersham, Arlington Heights,

IL) as we have previously described (*27*). A total of 2×10^5 cells were planted on 24-well plates and cultured for ~17−19 h before the experiments. The mean value of the data was fit to a sigmoid curve with a variable slope factor using the nonlinear least-squares regression in Graphpad Prism (Graphpad Software). EC_{50} values are reported as the mean ± standard error. Experiments were repeated at least 3 times using duplicate wells on different days.

Modeling of MCR−Antagonist Complexes. Homology models of ASIP(93−132) and MCRs can be generated automatically using various standard software (*30*−*32*) or taken from the ModBase database (*33*). However, because of low sequence homology between MCRs and rhodopsin (~15%), receptor models were identified as unreliable in ModBase (score of 0.02−0.1).

In this study, homology modeling and receptor−antagonist docking were accomplished using iterative distance geometry refinement, an approach that has been described and tested previously (*34*−*36*). The calculations were conducted using DIANA (*37*), QUANTA (Accelrys), and supplementary in house software for the generation of distance and angle constraints (*34*). The constraints were of several types. First, the backbone structure was restrained as in the corresponding experimental template (crystal structure of rhodopsin or NMR models of agouti-related peptides) by using the corresponding $C^\beta \cdots C^\beta$ distances with allowed deviations of 1 Å, as the upper distance constraints. This permits small structural adjustments during the calculations. Second, we included an evolving system of hydrogen-bonding constraints that was iteratively refined during the calculations, as described previously (*34*, *36*). These hydrogen bonds were formed within the receptors and peptides and between them. The upper distance constraints were 1.9 Å for H···O, 2.9 Å for O···O and N···O, 2.6 Å for H···S bonds, and 3.5 Å for O···N, participating in the binding of Zn^{2+} ions. For disulfide bonds, the upper limits for distance constraints were chosen as 2.04, 3.05 and 4.20 Å for $S^\gamma \cdots S^\gamma$, $C^\beta \cdots S^\gamma$, and $C^\beta \cdots C^\beta$ distances, respectively. Finally, the dihedral angles in α helices were constrained with allowed deviations of ±30°. Most of the side-chain conformers (χ angles) were "traced" as in the experimental templates, while others were adjusted during the iterative distance geometry refinement. The optimization protocol and weighting factors have been described previously (*34*).

The computations included three steps: (1) comparative model of ASIP(93−132), which demonstrates 50% homology to AGRP(87−132), using a higher quality NMR structure of AGRP(87−120) [1mr0 (*8*)] as a template for the first 34 residues and a second NMR model of a longer fragment AGRP(87−132) [1hyk (*18*)] as a template for the C-terminal loop 121−132, (2) homology modeling of MCR1 and MCR4, based on the crystal structure of rhodopsin (1gzm) (*26*), and (3) calculation of three receptor−antagonist complexes using our mutagenesis data to identify residues important for binding of ASIP(93−132) and AGRP(87−132) by the corresponding receptors.

The inactive conformation of hMC1R and hMC4R were modeled using the X-ray structure of the inactive state of rhodopsin with its bound inverse agonist 11-*cis* retinal. The corresponding sequence alignment is shown in Figure 1. The modeling of loops was a significant challenge. All short intracellular loops were modeled from the rhodopsin template, except for 4−5 extra residues in IL3, which were added as an α-helical extension of TMH5. The long extracellular loop EL1 was predicted to form a β hairpin, judging from its hydrophobicity pattern and the high β-sheet propensity of residues in this region. A similar β hairpin in EL1 exists in all bacterial rhodopsins, another family of seven α-helical transmembrane proteins. Therefore, this loop was modeled using the corresponding β hairpin from sensory rhodopsin (1gue, residues 56−71) as a structural template. The N-terminal segment of the receptors (before the conserved cysteine in the N terminus) and C-terminal segments, following helix 8, were omitted in the calculations. It has previously been shown that deletion of 23 N-terminal residues in hMC1R or 28 residues in hMC4R does not affect ligand binding (*38*). The three residues of EL2 (YYD in MC1R and YSD in MC4R) adopted an extended conformation during the calculations to connect ends of the adjacent TMH4 and TMH5. The structurally important EL3 was constrained by the ends of adjacent helices and by different combinations of disulfide bonds that could be formed within EL3 of MC4, as natural (271−277), "rescue" (272−277), or "improper" (271−279 and 277−279) disulfide bridges (ref *39* and this paper). The residues from the N terminus, preceding TMH1 (Figure 1), were restricted to an extended conformation, attached to EL3 by a disulfide bond, which was proposed from mutagenesis studies of MC1R (*42*). Suggesting the conservation of the disulfide bond system among MCRs and considering current and previously published experimental data (see the Results), we explicitly introduced two proposed native S−S bonds, one within EL3 and another between EL3 and the N terminus in each receptor (Cys^{271}−Cys^{277} and Cys^{40}−Cys^{279} in hMC4R and Cys^{267}−Cys^{273} and Cys^{35}−Cys^{275} in MC1R), while other cross-linking restraints were included as C^β−C^β distances of 5 and 7 Å between residues corresponding to "rescue" and "improper" S−S bond partners, respectively. Additionally, two alternative models of the hMC4R were calculated with different disulfide bond patterns, corresponding to the formation of "improper" bridges (*39*): one for the C271A mutant with the Cys^{277}−Cys^{279} bond and another for the C277A mutant with the Cys^{271}−Cys^{179} bond. Additional constraints were taken from a zinc-binding site that can be formed between TMHs 2 and 3 (I103H−Asp^{122}) of MC4R (*41*). All hydrogen bonds formed by the loops were also applied as distance constraints.

The initial docking of antagonists was accomplished manually (using QUANTA). The approximate arrangement of peptide and receptors was defined based on protein−protein interactions identified by site-directed mutagenesis in the current and previously published studies (*17*, *23*). Interactions between key residues, such as Arg-Phe-Phe in the peptide antagonists and acidic and aromatic residues in the transmembrane domains of both receptors (see Table 1), guided the initial ligand docking. The initial structure of the complex was then refined by iterative distance geometry calculations. The refinement was guided by the formation of intermolecular hydrogen bonds, between the receptors and Tyr^{109}, Arg^{111}, Asn^{114}, Tyr^{118}, and Arg^{120} of AGRP(87−132) or Glu^{115}, Arg^{117}, Arg^{120}, Ser^{121}, Ser^{124}, and Arg^{126} of AGRP-(93−132) and by side-chain packing at the protein−protein interface (Table 3). The likelihood of proposed hydrogen-bond contacts between polar atoms of the receptor and ligand

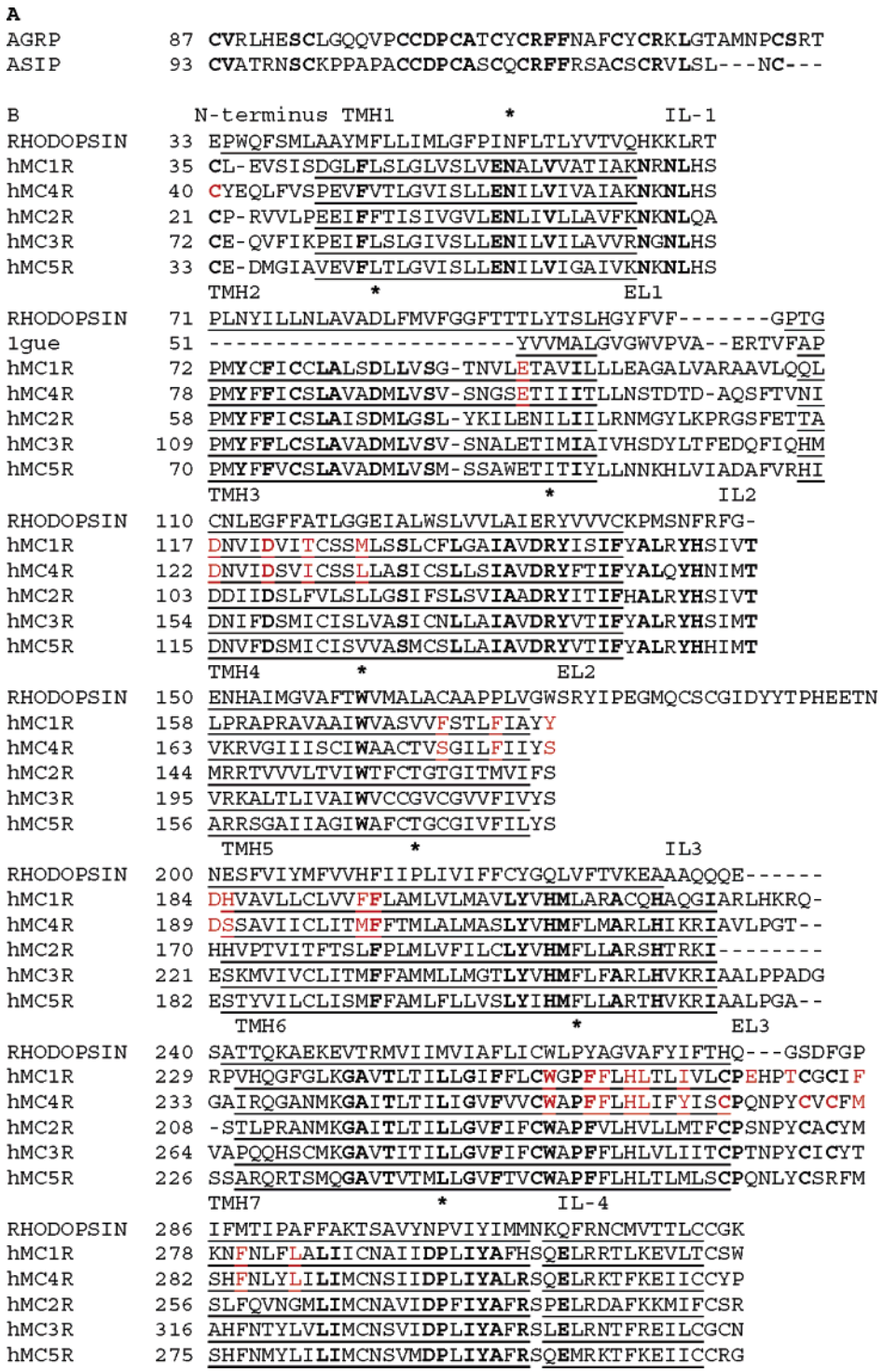

FIGURE 1: Sequence alignments of (A) AGRP(87−132) with ASIP(93−132) and (B) bovine rhodopsin with five human MCRs. Bold characters represent conserved (>95% identity for 154 MCRs) residues in MCRs and identical residues in both ligands. Underlined characters represent residues from α helices. Mutated residues are colored red. The most conserved residue in each TMH (1.50, 2.50, 3.50, 4.50, 5.50, 6.50, and 7.50 in the nomenclature of ref *59*) of rhodopsin-like GPCR is indicated with an asterisk.

taken from the manually docked complexes were subsequently modified during the iterative refinement procedure to satisfy the hydrogen-bonding potential of buried polar groups and to decrease the target function of the calculated complex. The constraints and the corresponding structure of the ligand−receptor complexes simultaneously evolved during refinement steps until the final structure satisfied the following criteria: target function of the complex was <50; pairwise root-mean-square deviation (rmsd) between the transmembrane part of the receptor in the complex and the transmembrane part of the receptor calculated alone was <1 Å (for 208 Cα atoms); and the rmsd between the ligand in the complex and the ligand calculated alone was <0.5 Å (for 40−46 atoms).

RESULTS

Antagonist Binding to hMC4R and hMC1R. To understand the molecular determinants of binding of natural peptide

Table 1: Competitive Displacements of ^{125}I-ASIP[90−132(L89Y)] and ^{125}I-AGRP (86−132) by the Corresponding Nonlabeled Peptides on Cells Expressing Human Wild-Type and Mutants MC1 and MC4 Receptors[a]

hMC4R				hMC1R		
receptor	B_{max} (fmol/mg)	AGRP(86−132) IC_{50} (nM)	ASIP[90−132(L89Y)] IC_{50} (nM)	receptor	B_{max} (fmol/mg)	ASIP[90−132(L89Y)] IC_{50} (nM)
hMC4R wild type	375 ± 35	2.1 ± 1.0	9.2± 1.3	hMC1R wild type	318 ± 38	8.5 ± 0.1
			Interactions Involving AGRP Arg^{111} or ASIP Arg^{117}			
E100A(TMH2)	327 ± 12	3.97± 0.1	**76.1 ± 4.2**	E94A(TMH2)	319 ± 16	**59.0 ± 4.1**
D122A(TMH3)	344 ± 13	1.5 ± 0.5	15.3 ± 1.3	D117A(TMH3)	194 ± 29	**91.6 ± 16.5**
D126A(TMH3)	290 ± 30	**38.5 ± 4.5**	**110.7 ± 2.0**	D121A(TMH3)	226 ± 30	**64.4 ± 15.2**
D122A/D126A	**175 ± 33**	**NB**	**148.0 ± 26.2**	D117A/ D121A	**103 ± 14**	**119.3 ± 0.5**
			Interactions Involving AGRP Phe^{112} or ASIP Phe^{118}			
I129A(TMH3)	329 ± 28	**8.4 ± 0.8**	**73.9 ± 5.5**	T124A(TMH3)	286 ± 19	**20.1 ± 1.5**
W258A(TMH6)	299 ± 21	2.3 ± 0.1	**44.6 ± 12.1**	W254A(TMH6)	337 ± 15	14.8 ± **2.5**
F284A(TMH7)	339 ± 22	1.7 ± 0.3	**104.6 ± 6.1**	F280A(TMH7)	289 ± 14	**50.1 ± 3.6**
L288A(TMH7)	379 ± 35	**6.0 ± 0.1**	21.0 ± 1.8	L284A(TMH7)	260 ± 22	**323 ± 12**
			Interactions Involving AGRP Phe^{113} or ASIP Phe^{119}			
L133A(TMH3)	417±16	1.0 ± 0.4	17.4 ± 0.5	M128A(TMH3)	349 ± 27	5.4 ± 0.6
S180F(TMH4)	273 ± 9	**7.0 ± 0.2**	**25.2 ± 0.2**	F175S(TMH4)	271 ± 25	4.5 ± 0.5
				F175A(TMH4)	317 ± 19	6.8 ± 0.4
M200A(TMH5)	365 ± 24	3.1 ± 0.1	5.9 ± 0.5	F195A(TMH5)	314 ± 15	3.4 ± 0.5
F201A(TMH5)	430 ± 21	4.2 ± 0.2	8.3 ± 0.5	F196A(TMH5)	286 ± 14	11.5 ± 1.1
F261A(TMH6)	361 ± 15	**10.2 ± 1.9**	5.4 ± 0.2	F257A(TMH6)	**131 ± 17**	**67 ± 6**
F262A(TMH6)	317 ± 22	1.4 ± 0.4	19.3 ± 0.8	F258A(TMH6)	315 ± 14	4.0 ± 0.3
F261A/F262A	**113 ± 16**	**121 ± 28**	**48.6 ± 2.5**	F257A/F258A	**107 ± 16**	**66.3 ± 10**
L265A(TMH6)	320 ± 19	**16.1 ± 1.8**	**75.7 ± 13.5**	L261A(TMH6)	321 ± 20	13.4 ± 3.2
			Interactions Involving AGRP Ala^{115} or ASIP Ser^{121}			
H264A(TMH6)	292 ± 10	4.7 ± 1.8	**107.1 ± 11.3**	H260A(TMH6)	221 ± 29	4.3 ± 1.6
			Interactions Involving AGRP Phe^{116} or ASIP Ala^{122}			
Y268A(TMH6)	321 ± 18	3.6± 1.8	6.5 ± 1.1	I264Y(TMH6)	321 ± 39	5.2 ± 0.6
M281F(EL3)	**77 ± 37**	**15 ± 6**	**154 ± 40**	F277M(EL3)	**170 ± 21**	**140 ± 16**
			Interactions Involving Receptor EL2 and EL3			
F184A(TMH4)	331 ± 26	1.05 ± 0.3	20.5 ± 1.1	F179A(TMH4)	255 ± 15	10.1 ± 0.4
S188Y(EL2)	266 ± 38	1.9 ± 0.2	5.3 ± 0.4	Y183S(EL2)	311 ± 19	**33.0 ± 2.6**
D189H(EL2)	371 ± 26	1.8 ± 0.3	6.0 ± 0.2	D184H(EL2)	280 ± 23	**41.2 ± 2.8**
S190H(EL2)	317 ± 18	2.5 ± 0.2	8.8 ± 0.7	H185S(EL2)	201 ± 14	**173 ± 27**
				E269Q(EL2)	335 ± 16	6.9 ± 0.4
				E269S(EL2)	356 ± 26	12.0 ± 1.3
				T272Y(EL2)	314 ± 22	7.6 ± 0.8
				D184H/E269S	272 ± 15	**61.3 ± 4.2**
				H185S/T272Y	304 ± 35	9.2 ± 0.5

[a] NB, no detectable binding. B_{max} values were calculated from ^{125}I-ASIP[90−132(L89Y)] displacement curves. Bold characters indicate the substantial changes in binding affinity (exceeding 3-folds) and the significant changes in receptor cell surface expression (B_{max} decreased more than 2 times).

Table 2: Effect of Mutagenesis of Conserved Cysteines from the N Terminus (Cys40) and EL3 (Cys271, Cys277, and Cys279) of hMC4R on the Binding Affinity of AGRP(86−132), ASIP[90−132(L89Y)], and NDP-MSH and on NDP-MSH-Induced cAMP Accumulation[a]

		IC_{50} (nM)			cAMP (NDP-MSH)			
hMC4R mutations	B_{max} (fmol/mg)	AGRP(86−132)	ASIP[90−132 (L89Y)]	NDP-MSH	EC_{50} (nM)	E_{max} (pmol)	fold (above basal)	possible S−S bonds
wild type	375 ± 35	2.1 ± 1.0	9.2 ± 1.3	2.3 ± 0.3	0.62 ± 0.06	34.03 ± 3.5	45.4	$C^{271}-C^{277}$ $C^{40}-C^{279}$
C40A(S1)	303 ± 20	2.6 ± 0.8	16.7 ± 1.3	5.4 ± 1.1	0.38± 0.12	30.6 ± 2.8	43.1	$C^{271}-C^{277}$
C271A(S2)	47 ± 6	NB	202 ± 45	NB		6.01 ± 2.2	7.5	$C^{277}-C^{279}$
C277A(S3)	134 ± 19	1.7 ± 0.4	30.3 ± 2.5	2.7 ± 0.8	2.6 ± 0.1	20.2 ± 3.6	21.7	$C^{271}-C^{279}$
C279A(S4)	358 ± 12	2.4 ± 0.3	11.8 ± 0.6	1.7 ± 0.13	0.61 ± 0.03	28.75 ± 4.5	41.7	$C^{271}-C^{277}$

[a] NB, no detectable binding observed using 0.35 nM of radioligand. The highest cold ligand concentration used was 10^{-6} M. Nonspecific was determined in the presence of cold ligand at 10^{-5} M. Basal cAMP levels can be calculated by dividing E_{max} by the fold (above basal). B_{max} values were calculated from ^{125}I-ASIP[90−132(L89Y)] displacement curves.

antagonists, we undertook comparative studies of the effects of equivalent point mutations in hMC1R and hMC4R on the binding affinity of ASIP or ASIP/AGRP, respectively. Corresponding residues of both receptors were mutated in TMHs 2−7, EL2, and EL3 in the area of the predicted ligand-binding pocket, previously defined for MC1R and MC4R using a large set of different melanocortin ligands (*17*, *23*, *27*, *42*). The results of competition binding assays of ASIP[90−132(L89Y)] and AGRP(86−132) against their radioactive analogues in the HEK 293 cells, expressing either the wild-type or mutated receptor of both types, are summarized in Table 1.

Importantly, several receptor mutations, such as double mutants of acidic residues in TMH3 (D122A/D126A in

Table 3: Hydrogen Bonds between Receptors and Antagonists in the Modeled Complexes of hMC1R−ASIP(90−132), hMC4R−ASIP(90−132), and hMC4R−AGRP(86−132)[a]

hMC4R−AGRP		hMC4R−ASIP		hMC1R−ASIP	
receptor	ligand	receptor	ligand	receptor	ligand
		Hydrogen Bonds Involving Receptor TMH2			
		Glu^{100} Oϵ1	Arg^{117} Nη1	**Glu^{94} Oϵ1**	Arg^{117} Nη1
		Hydrogen Bonds Involving Receptor EL1			
Asp^{113} Oδ1	Arg^{131} Nϵ				
		Asp^{111} O	Ser^{129} Oγ	Ala^{105} O	Ser^{129} Oγ
		Ala^{114} O	Arg^{97} Nη2	Arg^{109} O	Arg^{97} Nη2
Gln^{115} O	His^{91} Nϵ2	Gln^{115} O	Arg^{97} Nη2	Ala^{110} O	Arg^{97} Nη2
Thr^{118} Oγ1	Arg^{120} Nη2	Thr^{118} Oγ1	Arg^{126} Nη2	Gln^{115} Oϵ1	Arg^{126} Nη2
		Hydrogen Bonds Involving Receptor TMH3			
Asp^{122} Oδ1	Arg^{111} Nη1	Asp^{122} Oδ1	Arg^{117} Nη1	**Asp^{117} Oδ1**	Arg^{117} Nη1
Asp^{122} Oδ1	Arg^{111} Nϵ			**Asp^{117} Oδ1**	Arg^{117} Nϵ
Asn^{123} Oδ1	Tyr^{109} Oη				
Asp^{126} Oδ1	Arg^{111} Nη2	**Asp^{126} Oδ1**	Arg^{117} Nη2	**Asp^{121} Oδ1**	Arg^{117} Nη2
Asp^{126} Oδ1	Phe^{113} N				
		Hydrogen Bonds Involving Receptor EL2			
		Ser^{188} Oγ	Gln^{115} Oϵ1	**Tyr^{183}Oη**	Gln^{115} Oϵ1
Ser^{190} Oγ	Cys^{94} O	Ser^{190} Oγ	Pro^{104} O	**His^{185} Nδ1**	Cys^{100} O
Ser^{190} O	Gly^{96} N	Ser^{190} Oγ	Ala^{104} O	**His^{185} Nϵ2**	Cys^{114} O
		Asp^{189} O	Arg^{120} Nη1	Asp^{184} O	Arg^{120} Nη1
		Hydrogen Bonds Involving Receptor TMH6			
Leu^{265} O	Asn^{114} Nϵ2				
		His^{264} Nϵ2	Ser^{121} Oγ		
Tyr^{268} Oη	Ala^{115} O	Tyr^{268} Oη	Ser^{121} O		
		Hydrogen Bonds Involving Receptor EL3			
Pro^{272} O	Gln^{97} Nϵ2				
Asn^{274} O	Gln^{97} Nϵ2				
Asn^{274} Oδ1	Gln^{98} Nϵ2				
Tyr^{276} Oη	Ser^{93} Oγ	Tyr^{276} Oη	Ser^{99} Oγ	Thr^{272} Oγ1	Ser^{99} O

[a] Bold characters indicate mutated residues that significantly affected peptide antagonist binding. Only hydrogen bonds with N···O distances less than 3.2 Å were presented in Table 3. These hydrogen bonds were used for the automated docking of the antagonist in the corresponding receptors.

hMC4R or D117A/D121A in hMC1R), double mutants of aromatic residues in TMH6 (F261A/F262A in hMC4R or F257A/F258A in hMC1R), or single mutants in EL3 (M281F in hMC4R or F277M in hMC1R) demonstrated decreased B_{max} values (Table 1). The low B_{max} could be caused by a combination of low receptor expression and reduced ^{125}I-ASIP[90−132(L89Y)] binding affinity, and therefore it was corrected for K_d (see the Experimental Procedures). However, other mutants with similarly low IC_{50} (e.g., F284A in hMC4R) had B_{max} values similar to the wild-type receptors. This suggests that the major cause for reduced B_{max} values may be low cell-surface expression. We can suggest that these residues may also have an important structural role. The correct conformation of EL3, which can be damaged by a single-point mutation (M281F), seems to be particularly important for stabilization of a receptor structure that is able to bind ligands.

Our current data show that AGRP(86−132) binds only wild-type MC4R ($IC_{50} \sim 2$ nM), while ASIP[90−132-(L89Y)] interacts well with both wild-type hMC1R and wild-type hMC4R ($IC_{50} \sim 9$ nM). All designed mutants of both receptors, except the D122A/D126A double mutant of hMC4R, retained binding affinity for their corresponding ligands with variations in IC_{50} in the nanomolar range. However, no hMC1R mutant examined, including triple mutant F175S/F277M/H185S, acquired detectable AGRP-(87−132) binding (data not shown).

The comparison of the binding affinity of ASIP[90−132-(L89Y)] and AGRP(86−132) to the wild-type and mutated hMC4R allowed us to determine which residues from the receptor-binding pocket are important for high-affinity binding of both ligands, which residues have distinct effects on each peptide, and which residues are nonessential for binding. Changes in binding affinity exceeding 3-fold are shown in Table 1 in bold characters. Almost half of the single mutants demonstrated significant changes in the binding of one or both antagonists, which might suggest an involvement of these residues in direct contact with the corresponding ligands, although an indirect effect cannot be excluded. In general, ASIP[90−132(L89Y)] binding was affected by a greater number of single mutations. However, ASIP[90−132(L89Y)] binding was not eliminated by any of the mutations tested. In contrast, AGRP(86−132) binding was completely abolished in the D122A/D126A double mutant and largely impaired in the F261A/F262A double mutant. Residues whose mutation significantly influenced binding of both antagonists include Asp^{126}, Ile^{129}, Ser^{180}, Leu^{265}, and Leu ^{288} in TMHs 3, 4, 6, and 7 and Met^{277} in EL3. Residue replacements that impaired binding of only ASIP[90−132-(L89Y)] were E100A, W258A, F262A, H264A, and F284A in TMHs 2, 6, and 7. Other tested residues from the predicted binding pocket of hMC4R, including residues from EL2, were not essential for the binding of either antagonist. These data indicate that both antagonists share a similar binding pocket in hMC4R, where both ligands are in contact with residues from TM3, TM5, and TM6, while ASIP[90−132-(L89Y)] more strongly interacts with residues from TM2 (Glu^{100}) and TM7 (Phe^{284}).

In the second part of our mutagenesis studies, we sought to understand the distinction between hMC4R and hMC1R in binding ASIP[90−132(L89Y)]. Residues predicted to be involved in binding ASIP[90−132(L89Y)] in both receptors are localized in TMHs 2, 3, 4, 6, and 7 and EL3 (corresponding to Glu^{94}, Asp^{121}, Thr^{124}, Phe^{175}, Phe^{257}, Phe^{258}, Phe^{280}, and Leu^{284} of hMC1R). However, some dissimilarity in binding effects was observed in hMC1R, as compared with hMC4R, for several mutations in helices 3, 4, and 6 and particularly in EL2. For example, the D117A mutation in hMC1R demonstrated a larger negative effect, while W254A and L261A had a smaller impact on ASIP[90−132-(L89Y)] binding than did the corresponding substitutions in hMC4R. Interestingly, several mutations in hMC1R (M128A, F175S, F258A, and H264A) slightly increased the binding affinity of ASIP[90−132(L89Y)], while the homologous substitution in hMC4R (L133A, S180F, and F262A) significantly decreased its binding. On the other hand, mutations in TMH6 (F257A) and in EL2 (Y183S, D184H, and H185S) impaired binding of the antagonist to hMC1R, while the homologous mutations in hMC4R to some extent improved its affinity. These data suggest a dissimilar positioning of ASIP in both receptors, which may be attributed to the different geometries of their binding pockets.

Disulfide Bonds in the Structure of EL3 of hMC4R. MCRs lack the conserved disulfide bond between TMH3 and EL2, which participates in structural stabilization in numerous GPCRs (*43*). Therefore, in MCRs, other extracellular disulfides likely exist to maintain a correct receptor conformation. Recently, it was suggested that conserved cysteines from the N terminus (named here S_1), TMH6 (S_2), and EL3 (S_3 and S_4) of MC1R and MC4R could form structurally and functionally important disulfide bonds (*39*, *40*, *44*, *45*). However, the published data are conflicting, indicating the presence of one (*44*, *45*) or two (*40*) disulfide bonds and pointing to different cross-linking partners (*39*, *44*). In MC1R, an S_2-S_4 bond in EL3 was proposed (*46*) based on the similar functional phenotype of corresponding mutants. In MC4R, a different S_2-S_3 bond between TMH6 and EL3 was suggested as the native one, although the data obtained also indicated that, in a mutant receptor lacking S_2, abnormal disulfide bonds, S_3-S_4, could be formed and aggravate the damaging effect of a broken S_2-S_3 bond (*39*).

To understand the structural and functional roles of conserved extracellular cysteines, four cysteine−alanine substitutions were made in the N terminus (C40A), TMH6 (C271A), and EL3 (C277A and C279A) of hMC4R and the consequences of these mutations were examined. We compared the binding affinities of the agonist, NDP-MSH, and the antagonists, ASIP[90−132(L89Y)] and AGRP(86−132), at the wild-type and mutant hMC4Rs (C40A, C271A, C277A, and C279A). In addition we studied agonist-induced cAMP production.

The results (Table 2) indicate that mutation of S_2 cysteine, C271A, eliminates detectable AGRP(86−132) and NDP-MSH bindings and decreases the binding of ASIP[90−132-(L89Y)] ~20-fold. S_2 mutation also significantly interfered with the agonist-induced cAMP accumulation. A similar effect of the S_2 mutation has been observed for MC4R (*39*) and MC1R (*40*, *44*). Mutation of the S_3 cysteine, C277A, decreased the binding of ASIP[90−132(L89Y)] and affected the potency of receptor activation by NDP-MSH (~4-fold increase in EC_{50}). A similar effect of C277A has been reported for the activation of the MC4R mutant by MSH and β-MSH, while a stronger effect has been observed for NDP-MSH-induced activation (*39*). Moreover, both positions, S_2 and S_3, appear to be structurally important, because alanine substitutions for these cysteines decreased the B_{max} values, indicating an impaired level of cell-surface expression for these mutant receptors. In contrast, mutation of S_4 cysteine (C279A) demonstrated a wild-type-like phenotype, and the mutation of N-terminal S_1 cystein (C40A) had only a minor influence on the binding of ASIP[90−132(L89Y)] and NDP-MSH, while preserving the wild-type activation ability. This also agrees with published data for these MC4R mutants (*39*). Interestingly, the effects of similar mutations in MC1R were more controversial (*40*, *44*). In some experiments, mutation of the S_4 cysteine (C273A) severely damages MC1R activation by MSH, while the S_3 mutation (C271A) has a smaller effect (*44*). However, in another study of MC1R (*40*), the S_4 mutation has less of an effect on NDP-MSH binding than S_2, S_1, or S_3 mutations.

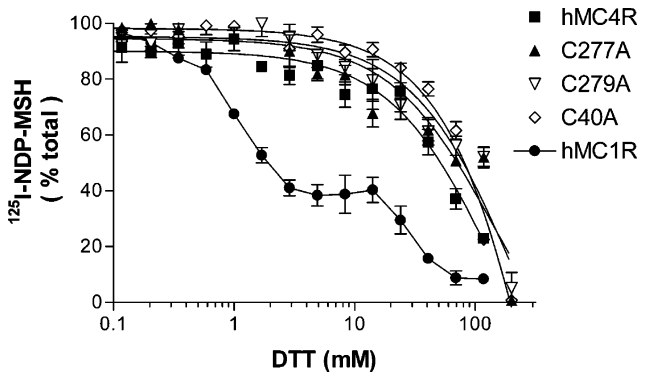

FIGURE 2: Effect of disulfide reduction by DTT on the binding of ^{125}I-NDP-MSH to the wild-type human MC1 and MC4 receptors and MC4 mutants with alanine replacement for the conserved cysteines (C40A, C277A, and C279A).

To further examine extracelluar disulfides in the MCRs and to deduce the possible disulfide bond partners, we studied the effect of disulfide reduction by dithiothreitol (DTT) on the binding affinity of NDP-MSH in cysteine mutants. Each antagonist, ASIP[90−132(L89Y)] and AGRP(86−132), has 5 disulfide bonds and thus is not appropriate for use as a ligand in the presence of DTT. Therefore, ^{125}I-NDP-MSH was chosen for binding experiments in the presence of DTT (1−100 mM) with wild-type hMC1R and hMC4R and C40A, C277A, and C279A hMC4R mutants (Figure 2). DTT dependence could not be assessed for the C271A mutant, which did not have detectable binding of NDP-MSH (Table 2).

In wild-type hMC1R, DTT decreased ^{125}I-NDP-MSH binding in a biphasic manner with IC_{50} values of 2 and 30 mM DTT, in agreement with previous observations (*40*). The biphasic character of the DTT titration curve suggests the presence of two disulfide bonds. One disulfide is fully reduced at 10 mM DTT, decreasing agonist binding by 60%, while the second is fully reduced at 100 mM DTT, leading to complete loss of NDP-MSH binding. In contrast, hMC4R demonstrated a monophasic DTT behavior for the wild-type and three cysteine mutants (C40A, C277A, and C279A). Interestingly, all hMC4R variants were DTT-sensitive with a similar IC_{50} ~ 60 mM. These data suggest that the wild-

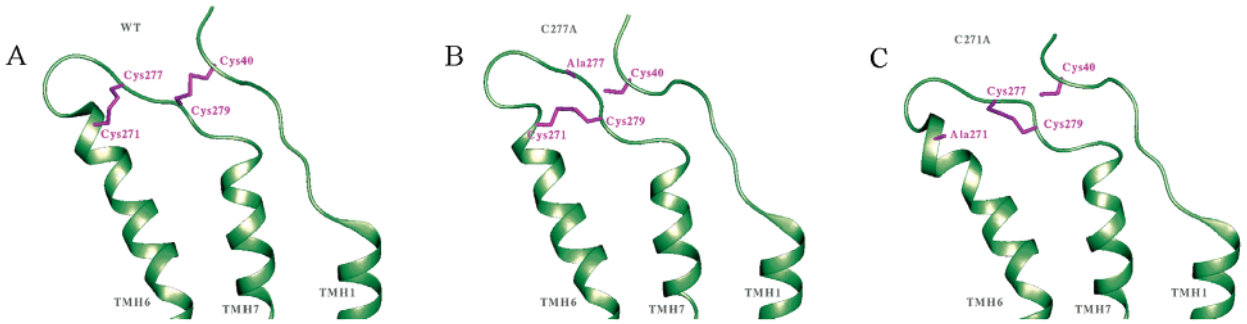

FIGURE 3: Disulfide bonds in the model of hMC4R (A), Cys^{40}−Cys^{279} and Cys^{271}−Cys^{277}; in C277A mutant of hMC4R (B), Cys^{271}−Cys^{279}; and in C271A mutant of hMC4R (C), Cys^{277}−Cys^{279}. The EL3, part of N termunus, and helices 1, 6, and 7 are shown by ribbons. The conserved cysteines and alanines substituted for Cys^{277} (B) and Cys^{271} (C) are colored purple.

type hMC4R and hMC4R mutants (C40A, C277A, and C279A) have at least one S−S bond, which is important for high-affinity NDP-MSH binding and can be reduced only at a high DTT concentration.

Modeling of Antagonist ASIP(93−132) and Two MCRs, hMC1R and hMC4R. The computational part of this study included homology modeling and docking of water-soluble peptide ligands with transmembrane receptors. ASIP(93−132) was calculated by distance geometry from structures of its close homologue, AGRP (PDB entries 1mr0 and 1hyk), as described in the Experimental Procedures. The calculated structure of ASIP(93−132) was well-defined, with a pairwise rmsd < 0.40 Å (for 40 C^{α} atoms) within a set of 50 models with the lowest target function. The five best models had an rmsd of 0.8−1.0 Å (for 28 C^{α} atoms) with the original template, AGRP(87−120) (excluding the N-terminal loop). This is comparable to the deviations in backbone coordinates between two NMR structures of the AGRP fragments, 1hyk and 1mr0 (rmsd of 1.14 Å for 28 C^{α} atoms). The proline-rich N-terminal loop of ASIP, ^{100}CKPPAPAC^{107}, was unconstrained during calculations. However, because of the presence of rigid proline residues, its backbone structure was unequivocally defined as $\beta\alpha_R\alpha_R\beta\alpha_R\beta\alpha_R\beta$ (where α_R and β denote regions of the Ramachandran plot occupied by the corresponding residues). The φ and ψ angles of residues in the N-terminal loop of ASIP(93−132) were constrained in these regions during calculations of receptor−ligand complexes. The model of AGRP(87−132) was obtained similarly. The distance geometry calculations produced a set of 50 structures with pairwise rmsd < 0.4 Å. The five best models had an rmsd of 0.8 Å with the 1mr0 template and 1.1 Å with 1hyk (excluding the N-terminal loop ^{122}LGQQVP^{128}, which has a different conformation in 1hyk). The conformation of the N-terminal loop of AGRP(87−132) was chosen as in 1mr0, because it permitted the formation of many more hydrogen bonds with the receptor (see Table 3).

The seven α-helical domains of the hMC1R and hMC4R receptors were modeled using the crystal structure of bovine rhodopsin (1gzm), as described in the Experimental Procedures. The most serious problem appears to be due to the presence of α-aneurisms in TMHs 2 and 5 of the rhodopsin template (*25*, *47*), which is unlikely to be a conserved feature in all GPCR structures (*36*). The α-aneurism represents the insertion of a single residue in an α-helical turn and is characterized by the formation of two hydrogen bonds of type *i* and *i* + 5 (*48*). A misalignment in the area of such insertions is detrimental for modeling, because this would produce a register shift in the TMH. The existence of α-aneurisms in TMHs 2 and 5 of MCRs can be deduced from the mutagenesis data (*17*, *23*, *27*), which indicate the importance of a conserved Glu in TMH2 and Phe^{195} (MC1R) or Met^{200} (hMC4R) in TMH5 for ligand binding and receptor activation. These residues are oriented into the binding pocket only if the rhodopsin-like α-aneurism is absent in TMH2 but preserved in TMH5. Therefore, the α-aneurism was removed from TMH2 and retained in TMH5.

During the modeling, we paid particular attention to the second (EL2) and third (EL3) extracellular loops (see the Experimental Procedures), because these loops are important for ligand binding, as is evident from our current (Table 1) and previously published (*15*, *22*) data. The conserved extracellular cysteine residues were oriented toward each other to allow the formation of two native disulfides (Cys^{35}−Cys^{275} and Cys^{267}−Cys^{273} in hMC4R and Cys^{40}−Cys^{279} and Cys^{271}−Cys^{277} in hMC4R) and to permit suggested rearrangement of disulfide bonds in the mutant receptors (*39*). The 10 best structures of each receptor, hMC1R and hMC4R, were well-defined with pairwise rmsd < 1 Å for all 283 (for hMC1R) or 282 (for hMC4R) C^{α} atoms. Larger deviations were observed for TMH5, near the ends of helices and in the loop regions. The models of hMC1R and hMC4R can be superimposed well with rhodopsin (1gzm): the corresponding rmsd values were ∼1.55 and 1.31 Å, respectively (for 198 common C^{α} atoms in TMHs). The imposed restrictions uniquely defined the conformation of EL3 of hMC4R, resulting in models with pairwise rmsd of 0.9 Å for C^{α} atoms (Figure 3A).

To examine whether the non-native disulfides (Cys^{271}−Cys^{279} and Cys^{277}−Cys^{279}) are actually possible in the C277A and C271A mutants of hMC4R (Table 2), we calculated models of these mutants with the alternative disulfides (parts B and C of Figure 3). In the C277A mutant, the structure of EL3 was nearly unchanged (rmsd from the wild-type of only 1.8 Å for 11 C^{α} atoms). However, in the C271A mutant, this loop was very flexible (rmsd of 3.27 Å within the set of generated conformations) and different from that in the wild-type protein (rmsd up to 4.7 Å) because of a sharp turn induced by cross-linking Cys^{277}−Cys^{279}. Thus, the non-native disulfide bridges can easily be formed in our models of the MCRs. Moreover, the minor conformational changes of EL3 in the C277A mutant are consistent with its small impair-

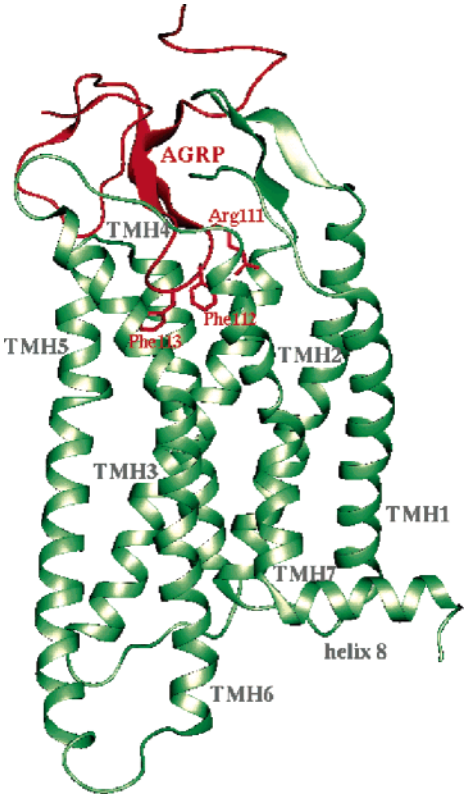

FIGURE 4: Model of the hMC4R−AGRP(87−132) complex. Receptor helices are shown as green ribbons, and the ligand is shown as a red cartoon. The conserved pharmacophoric element Arg[111]-Phe[112]-Phe[113] is shown by licorice-colored red.

ment, while the significant changes and flexibility of EL3 in the C271A mutant correlate with the observed misfolding and malfunction of the mutant (Table 2).

Modeling of Receptor−Antagonist Complexes. The models of hMC1R and hMC4R have an open cavity between TMHs 2−7, which is only partially covered by the N-terminal loop and EL1 and EL3. This cavity is large enough to accommodate small proteins, such as ASIP or AGRP. The receptor−antagonist docking was accomplished by distance geometry calculations, which were guided by hydrogen bonds applied as distance constraints. The set of hydrogen bonds was gradually refined (see the Experimental Procedures). The final sets of hydrogen bonds in the complexes (Table 3) were sufficient to uniquely define positions of the ligands: the deviations of their spatial positions were 1.5, 1.1, and 0.9 Å in the AGRP−hMC4R, ASIP−hMC4R, and ASIP−hMC1R complexes, respectively, in the sets of distance geometry generated structures (the corresponding rmsd values were calculated for atoms of the ligands, after superimposing only the receptors). Importantly, the association with ligands did not significantly affect the structures of the receptors: rmsd values between the ligand-bound and ligand-free receptors were in the range of 0.7−1.3 Å.

The mode of ligand binding is represented in Figure 4. All ligands are arranged similarly, with their common pharmacophore fragment Arg-Phe-Phe inserted deep between TMHs: Arg interacts with acidic residues in TMH2 and TMH3, and the first Phe interacts mostly with TMH3 (Thr[124] or Ile[129] in hMC1R and hMC4R, respectively) and TMH7 (Phe[280] or Phe[284] and Leu[284] or Leu[288]), while the second Phe occupies a site between TMH4 (Phe[175] or Ser[180]), TMH5 (Phe[195] or Met[200]), and TMH6 (Phe[257] or Phe[261], Phe[258] or Phe[262], and Leu[261] or Leu[265]). In the complexes, the N-terminal loop of the ligands forms a number of hydrogen bonds with EL2 and EL3, while their C-terminal loop and His[97] interact with EL1. The core octapeptide of AGRP(110−117) interacts not only with the transmembrane part of the receptor but also with residues in EL3 (Phe[280] and Met[281]). The specificity of binding largely depends on Ala[115] and Phe[116] of AGRP, which are replaced by Ser[121] and Ala[122] in ASIP. These residues of ASIP are close to Ile[276] and Phe[277] from EL3 of hMC1R.

The residues surrounding the key loop Arg[111]-Phe[112]-Phe[113] of AGRP(87−132) are shown in more detail in Figure 5, and the corresponding $C^{\beta}-C^{\beta}$ distances are presented in Table 4. The superposition of three ligand−receptor complexes reveals that the exact positions of the ligands vary slightly in the models. For example, ASIP(93−132) is shifted by ~1 Å relative to AGRP(87−132) in the complex with hMC4R. ASIP(93−132) moves toward TMH2 and TMH7, judging from the decreased distances between Arg-Phe and Glu[100] and Phe[284]. This correlates with the increased importance of the Glu[100] and Phe[284] residues of hMC4R for binding of the ASIP fragment (Table 1). Moreover, Ser[121] of ASIP approaches His[264] in TMH6 (distance changes by 1.5 Å), enabling the formation of an intermolecular hydrogen bond. This correlates with the increased influence of the H264A mutation on binding of the ASIP fragment to hMC4R (Table 1). In hMC1R, ASIP is shifted even further relative to its position in hMC4R. The interaction of the bulky Phe[175] from TMH4 with Phe[119] of ASIP(93−132) and the close contact between His[185] of hMC1R and the ligand N-terminal loop and 2 disulfides (100−114 and 116−123) promote the ~15° counterclockwise rotation (as viewed from the extracellular surface) of the entire ligand inside the binding pocket (Figure 6). The ligand movement in hMC1R relative to its position in hMC4R decreases the distance between Ala[122] of ASIP and Phe[277]-Met[281] of the receptors by ~2 Å (Table 4). The superposition of ASIP(93−132) in both receptors results in an rmsd of 2.29 Å for all 40 C^{α} atoms of the ligand, while a similar superposition of unbound ligands gives an rmsd of 0.86 Å for 40 C^{α} atoms. If the AGRP fragment was similarly positioned in the ligand-binding pocket of hMC1R, its Phe[116] residue would collide with Phe[277]. These hindrances may explain the observed poor binding of AGRP(86−132) to hMC1R.

DISCUSSION

The goal of this study was to identify the molecular determinants of binding affinity of AGRP(86−132) and ASIP(93−132) to hMC4R and hMC1R, using site-directed mutagenesis and molecular modeling. The obtained mutagenesis results together with published data were used to develop atomic models of hMC1R−ASIP(93−132), hMC4R−AGRP(86−132), and hMC4R−ASIP(93−132), which were helpful to better understand the experimental data.

Earlier point-mutation experiments (*17*, *23*) demonstrated the negative influence of E100K, D122R, D125A,N,K, D122A,N/D126A,N, F184K, Y187C, F201S, and F262S mutations on the binding affinity of AGRP fragments to MC4R; however, the binding interactions of ASIP with either MC1R and MC4R have not previously been examined.

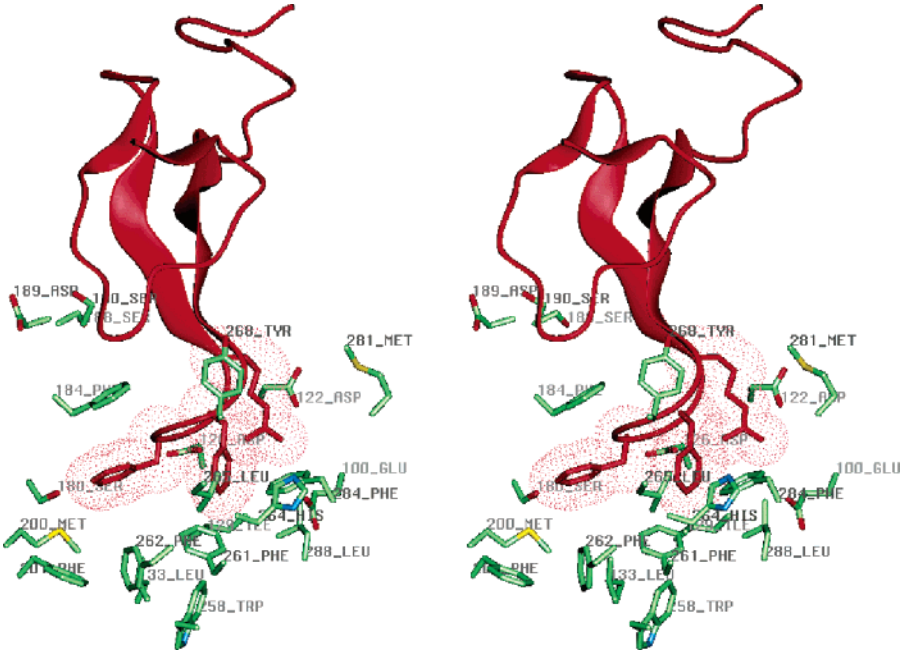

FIGURE 5: Stereoview of AGRP(87−132) inside hMC4R-binding pocket. Mutated residues of hMC4R are shown colored by element. AGRP(87−132) and pharmacophore element Arg^{111}-Phe^{112}-Phe^{113} are colored red.

Table 4: C^{β}−C^{β} Distances between Mutated Residues of Receptors and Antagonist Residues, Derived from the Modeled Complexes of hMC1R−ASIP(90−132), hMC4R−ASIP(90−132), and hMC4R−AGRP(86−132)[a]

hMC4−AGRP			hMC4R−ASIP			hMC1R−ASIP		
receptor residues	ligand residues	C^{β}−C^{β} distances (Å)	receptor residues	ligand residues	C^{β}−C^{β} distances (Å)	receptor residues	ligand residues	C^{β}−C^{β} distances (Å)
			Interactions Involving AGRP Arg^{111} or ASIP Arg^{117}					
Glu^{100}	Arg^{111}	11.9	**Glu^{100}**	Arg^{117}	**11.0***	**Glu^{94}**	Arg^{117}	**12.0***
Asp^{122}	Arg^{111}	4.9*	Asp^{122}	Arg^{117}	4.8*	**Asp^{117}**	Arg^{117}	**6.2***
Asp^{126}	Arg^{111}	**6.9***	**Asp^{126}**	Arg^{117}	**6.4***	**Asp^{121}**	Arg^{117}	**6.6***
			Interactions Involving AGRP Phe^{112} or ASIP Phe^{118}					
Ile^{129}	Phe^{112}	8.4	**Ile^{129}**	Phe^{118}	**7.9**	**Thr^{124}**	Phe^{118}	**8.1**
Trp^{258}	Phe^{112}	13.5	**Trp^{258}**	Phe^{118}	**13.6**	Trp^{254}	Phe^{118}	14.2
Phe^{284}	Phe^{112}	9.0	**Phe^{284}**	Phe^{118}	**8.0**	**Phe^{280}**	Phe^{118}	**7.6**
Leu^{288}	Phe^{112}	**8.9**	Leu^{288}	Phe^{118}	8.1	**Leu^{284}**	Phe^{118}	**8.3**
			Interactions Involving AGRP Phe^{113} or ASIP Phe^{119}					
Leu^{133}	Phe^{113}	8.1	Leu^{133}	Phe^{119}	8.1	Met^{128}	Phe^{119}	8.2
Ser^{180}	Phe^{113}	**8.8**	**Ser^{180}**	Phe^{119}	**9.5**	Phe^{175}	Phe^{119}	9.4
Met^{200}	Phe^{113}	9.7	Met^{200}	Phe^{119}	10.2	Phe^{195}	Phe^{119}	10.1
Phe^{201}	Phe^{113}	11.3	Phe^{201}	Phe^{119}	11.7	Phe^{196}	Phe^{119}	12.0
Phe^{261}	Phe^{113}	**9.0**	Phe^{261}	Phe^{119}	7.6	**Phe^{257}**	Phe^{119}	**8.3**
Phe^{262}	Phe^{113}	9.6	Phe^{262}	Phe^{119}	9.3	Phe^{258}	Phe^{119}	9.4
Leu^{265}	Phe^{112}	**6.9**	**Leu^{265}**	Phe^{118}	**5.5**	Leu^{261}	Phe^{118}	5.2
			Interactions Involving AGRP Ala^{115} or ASIP Ser^{121}					
His^{264}	Ala^{115}	8.8	**His^{264}**	Ser^{121}	**7.3***	His^{260}	Ser^{121}	8.4
			Interactions Involving AGRP Phe^{116} or ASIP Ala^{122}					
Tyr^{268}	Phe^{116}	9.3	Tyr^{268}	Ala^{122}	8.3	Ile^{264}	Ala^{122}	9.7
Met^{281}	Phe^{116}	**9.5**	**Met^{277}**	Ala^{122}	**9.5**	**Phe^{277}**	Ala^{122}	**7.7**
			Interactions Involving Receptors EL2 and EL3					
Phe^{184}	Phe^{113}	7.2	Phe^{184}	Phe^{119}	8.2	Phe^{179}	Phe^{119}	9.4
Ser^{188}	Tyr^{109}	7.2	Ser^{188}	Gln^{115}	5.7*	**Tyr^{183}**	Gln^{115}	**7.1***
Asp^{184}	Cys^{94}	9.6	Asp^{184}	Ala^{104}	7.6	**Asp^{184}**	Ala^{104}	**7.6**
Ser^{190}	Cys^{94}	4.7	Ser^{190}	Cys^{100}	4.6	**His^{185}**	Cys^{100}	**7.0**
						His^{185}	Cys^{114}	**8.0**
						His^{185}	Cys^{116}	**7.7**
						His^{185}	Cys^{123}	**7.0**
						Thr^{272}	Ser^{99}	**3.9***

[a] Bold characters indicate mutated residues that significantly affected peptide antagonist binding. An asterick indicates residues forming a hydrogen bond between side chains.

Consequently, we examined the binding affinity of ^{125}I-ASIP-[90−132(L89Y)] toward wild-type hMC1R and 30 of its mutants and the binding of both ^{125}I-ASIP[90−132(L89Y)] and ^{125}I-AGRP(86−132) toward wild-type hMC4R and 27

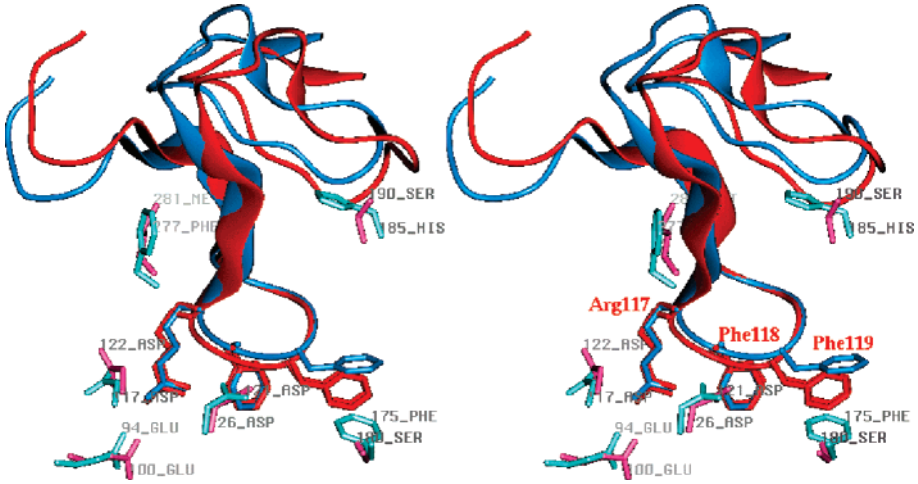

FIGURE 6: Stereoview of the superposition of modeled complexes: ASIP(93−132)−hMC1R (colored dark and light blue) and ASIP(93−132)−hMC4R (colored red and pink). Pharmacophore element of ASIP(93−132), Arg^{117}-Phe^{118}-Phe^{119}, a set of important residues of hMC1R (Glu^{94}, Asp^{117}, Asp^{122}, Phe^{175}, His^{185}, and Phe^{277}), and correspondent residues of hMC4R (Glu^{100}, Asp^{122}, Asp^{126}, Ser^{190}, Ser^{190}, and Met^{281}) are shown by licorice.

of its mutants in similar experimental conditions. The mutagenesis results indicate that the binding pockets of both ligands are composed of residues from homologous structural positions; however, similar mutations in different receptors affected the binding of both ligands slightly different (Table 2). These results can be attributed to the variations in positioning of different antagonists inside the ligand-binding pocket of both receptors.

To explain our experimental results, we performed modeling of the three receptor−ligand complexes. To improve the accuracy of the modeling and to avoid the common modeling errors related to the structural misalignment and erroneous loop modeling (*30*, *49*), we used model refinement by satisfying structural restraints (*31*). The restraints were derived not only from the structural templates (1gzm for the receptor and 1hyk and 1mr0 for the ligand) but also from mutagenesis experiments demonstrating the formation of Zn^{2+}-binding sites in MCRs (*39*−*41*, *44*). The native and non-natural disulfide bonds, which can be formed in wild-type or mutant receptors, provide the additional structural restrains.

The comparison of the three calculated receptor−antagonist models, hMC1R−ASIP(93−132), hMC4R−ASIP-(93−132), and hMC4R−AGRP(87−132), allows a better understanding of the specificity of receptor−ligand interactions. The major difference between binding pockets of the two receptors is associated with the presence of bulky Phe^{175} in TMH4, Phe^{195} in TMH5, His^{185} in EL2, and Phe^{277} in EL3 of hMC1R, which correspond to the smaller Ser^{180}, Met^{200}, Ser^{190}, and Met^{281}, respectively, in hMC4R. The interaction of the ligand with these residues results in a small rotation and ∼1 Å shift of ASIP toward TMH2 and TMH7 in the binding pocket of hMC1R, relative to its position and the position of the AGRP fragment in hMC4R (Figure 6). This altered positioning of the antagonists is consistent with the mutagenesis data presented in Tables 1 and 4.

In this study, we also tried to clarify the situation with suggested extracellular disulfide bonds that might exist in MCRs (*39*, *40*, *44*), using both mutagenesis and the modeling approach. Both MCRs, hMC1R and hMC4R, have 14 cysteines in TMHs and connecting loops. Four extracellular cysteines are highly conserved in this receptor subfamily: one in the N terminus (35 or 40 in hMC1R and hMC4R, respectively, denoted here as S_1), one in TMH6 (267 or 271, respectively, denoted here as S_2), and two in EL3 (273, 275 or 277, 279, respectively, denoted here as S_3 and S_4).

One of them, Cys^{271} (S_2) in hMC4R was shown to be highly functionally important, and its naturally occurring mutations (C271R and C271Y) are related to severe familial obesity (*46*, *50*, *51*). Previous results from cysteine mutagenesis in hMC4R indicated the involvement of Cys^{271} in a structurally and functionally important disulfide between TMH6 and EL3 (Cys^{271}−Cys^{277}) and provided evidence in favor of disulfide rearrangements inside EL3 in the mutant receptors (*39*). Interestingly, a similar situation was explored for the conserved disulfide bond between TMH3 (Cys^{110}) and EL2 (Cys^{187}) in bovine rhodopsin (*43*, *52*). The conserved disulfide Cys^{110}−Cys^{187} is required for correct folding and function of rhodopsin; however, in the naturally occurring mutants, C110F, C110Y, and C187Y, associated with retinitis pigmentosa, alternative disulfides were observed between Cys^{185}−Cys^{187} in EL2 (for C110F and C110Y) and between Cys^{110}−Cys^{185} (for C110F and C110Y) (*45*). It was shown, that the formation of the abnormal Cys^{185}−Cys^{187} disulfide causes receptor misfolding and loss of function, while in the C187A mutant, the formation of the Cys^{110}−Cys^{185} bond results in a wild-type-like phenotype with altered bleaching behavior.

The data presented in Table 2 and Figure 2 provide additional experimental evidence for the presence of two functionally important disulfide bonds in hMC1R and at least one important disulfide bond in hMC4R and its cysteine mutants (C40A, C277A, and C279A). A major question relates to the identification of disulfide bonds formed in the studied cases. Our results on hMC4R are in agreement with previously published data (*39*) that suggest that the native disulfide bridge is formed between Cys^{271} (S_2) and Cys^{277} (S_3), because in our experiments, C271A and C277A both affect the receptor expression level, ligand binding, and receptor activation, albeit to different extents. An additional S−S bond might be formed in wild-type hMC4R only between Cys^{40} (S_1) and Cys^{279} (S_4). However, C40A and

C279A mutants, where the S_1-S_4 bond is obviously absent and S_2-S_3 is preserved, demonstrate a wild-type-like phenotype. This result could indicate that the S_1-S_4 bond is less important for stability and activation of the wild-type hMC4R. However, minor changes in ligand binding for the C40A mutant (Table 2) suggest that such a disulfide bond is indeed likely present in the wild-type MC4R.

The sequence similarity of MCRs indicates that a common pattern of intramolecular disulfide bridges could be conserved throughout the receptor subfamily. The notable exception is hMC5R, which lacks the S_1-S_4 disulfide bond, because its S_4 cysteine is substituted by arginine (see Figure 1). Interestingly, hMC5R is characterized by unusually low affinity for MSH, but the Arg271 → Cys mutation, which could restore the S_1-S_4 disulfide bond, increases its affinity for MSH 690-fold (*53*). On the basis of sequence similarity of receptors and the biphasic behavior of the DTT titration curve (Figure 2), we suggest that hMC1R has two disulfides in homologous positions: $Cys^{35}-Cys^{275}$ and $Cys^{267}-Cys^{273}$. The S_1-S_4 bond may be more significant in hMC1R than in hMC4R, because its reduction by DTT (Figure 2) and its elimination by S_1 and S_4 mutations exhibited greater effects on the binding and activation characteristics of MC1R (*40*, *44*). We can also hypothesize that the S_1-S_4 bond is more reactive toward DTT, because it can be reduced at 10 mM DTT, leading to partially decreased NDP-MSH binding. In contrast, the complete loss of NDP-MSH binding only at 100 mM DTT for wild-type hMC1R and hMC4R and C40A and C279A mutants of hMC4R (Figure 2) indicates that the important S_2-S_3 bond, which is reduced in this case, is less reactive to DTT.

The organization of S−S bonds in the functionally impaired C271A and C277A mutants may be more complex. Neither of these mutants can form an S_2-S_3 bond. The C277A mutant still contains one disulfide bond that is reduced by 100 mM DTT (Figure 2), leading to decreased agonist binding. This disulfide in the C277A mutant could be either the native S_1-S_4 or a non-native S_2-S_4, if rearrangement of disulfides indeed takes place in the extracellular loops, as was previously suggested (*39*). The fact that the disulfide in the C277A mutant was reduced only at 100 mM DTT suggests the formation of the S_2-S_4 bond in place of the more DTT-reactive S_1-S_4 disulfide. Finally, the existence of an S−S bond in the functionally deficient C271A mutant could not be directly deduced from our data. However, our results do not contradict the recent suggestion that an improper S_3-S_4 disulfide, altering the receptor structure, could be formed in this case, causing the loss of function in the C271A mutant (*39*).

The disulfides in MCRs could play a similar role in structure stabilization as the conserved disulfide between TMH3 and EL2 in other GPCRs. The structural role of these disulfides in MCRs was also supported by distance geometry calculations (Figure 3). The modeling indicates that the C277A mutant of hMC4R, demonstrating a wild-type-like phenotype, has an alternative $Cys^{271}-Cys^{279}$ (S_2-S_4) bond that does not change the conformation of EL3, which in the wild-type receptor is stabilized by two disulfides: $Cys^{271}-Cys^{277}$ (S_2-S_3) and $Cys^{40}-Cys^{279}$ (S_1-S_4). In contrast, EL3 in the model of the C271A mutant with the abnormal $Cys^{277}-Cys^{279}$ (S_3-S_4) bond is highly flexible and has an altered conformation, which correlates with impaired receptor expression, ligand binding, and receptor activation in this mutant (Table 2).

Our models of hMC1R and hMC4R in complexes with their peptide antagonists differ in many details from recently published 3D models of MCRs (*24*, *41*, *54*) and dozens of automatically generated models that have been deposited in the GPCRDB (*55*) and ModBase databases (*33*), which also were based on the crystal structure of bovine rhodopsin. First of all, the sequence alignments with rhodopsin are often dissimilar in the area of loops and even in TMHs. For example, some automated models in GPCRDB and ModBase have misalignments in TMH5 or TMH7. Existing automated models (*33*) and several published MCR models (*41*, *54*) retain an α-aneurism in TMH2, which is present in the rhodopsin structure but absent in the μ-opioid receptor (*36*) and highly unlikely for MCRs. For example, in the hMC4R model proposed by Lagerström et al. (*41*), the presence of an α-aneurism in TMH2 forces the orientation of the functionally important Glu^{100} and two residues located one turn apart from Glu^{100} in TMH2 (Ile^{103} and Ile^{104}) toward the lipid bilayer. However, Glu^{100} is known to be important for binding of agonist and antagonists (Table 1) (*17*, *23*), and it can participate in the formation of the metal-binding site between TMH2 and TMH3 (*43*). To satisfy the experimental constraints between TMHs 2 and 3 derived from artificially designed Zn^{2+}-binding sites (Glu^{100}-I125H, Asp^{122}-I104A, or Asp^{122}-I103H), the authors proposed a 76° rotation of the central TMH3 (*41*), which dramatically modified the receptor structure relative to the rhodopsin template. In our model of hMC4R, which lacks an α-aneurism in TMH2 and is very similar to the rhodopsin template (rmsd of 1.31 Å for TMHs), Glu^{100}, Ile^{103}, and Ile^{104} face the ligand-binding pocket and at the same time are close enough to Asp^{122} and Ile^{125} in TMH3 to form a zinc-binding cluster.

The orientation of Glu^{100} toward the binding pocket was also proposed in the model of the MC4R−AGRP complex that has been developed recently by Haskell-Luevano and co-workers (*24*). Their receptor model is very similar to our model of hMC4R, with rmsd of 1.8 Å for 216 C^{α} atoms in TMHs. Moreover, the positions of the pharmacophore triplet Arg-Phe-Phe of AGRP(87−132) inside the ligand-binding pocket of the receptor are very close in both models. However, the bulk of AGRP is more tilted toward EL1 and TMH1 in the published model (*24*) relative to our model, resulting in an rmsd of 11.5 Å for 46 C^{α} atoms of the ligands after superimposing receptors of the modeled complexes. This demonstrates difficulties related to the correct docking of the ligands that should be guided not only by the interaction of the Arg-Phe-Phe triplet with the few aromatic and acidic residues of the receptor core but also by the interaction with the receptor loops. The ligand orientation in our models of hMC1R−ASIP, hMC4R−ASIP, and hMC4R−AGRP complexes was automatically generated by implementing the set of hydrogen-bond constraints between homologous residues from the receptor core and loops and ligand residues in all three cases (Table 3). Moreover, AGRP positioning in hMC4R is also restricted by the formation of the $Cys^{40}-Cys^{279}$ disulfide, which brings the N-terminal segment of the receptor close to EL3, and by the interactions with the extracellular loops. Finally, our modeled complexes better satisfy the known data on involvement of EL2 and EL3, rather than EL1, in ligand binding (*22*) and better

correlate with the significance of 27 homologous residues in the binding pocket of both receptors, hMC1R and hMC4R, for the antagonist binding results in Tables 1 and 4. In particular, our model explains the role of Phe^{175}/Ser^{180} in TMH4 for ligand binding, which in both receptors is in direct contact with the second Phe of the pharmacophore triplet of the peptide antagonists.

CONCLUSIONS

Because of experimental difficulties in crystallization of membrane proteins, comparative modeling using experimentally derived structural restraints (*31*) remains an important tool for understanding the molecular determinants of ligand−receptor interactions and to explain experimental results. Herein, for the first time, we have performed comparative studies of the binding of ASIP and AGRP fragments to both hMC1R and hMC4R. We modeled the complexes of hMC1R and hMC4R with their selective peptide antagonists ASIP-(97−132) and AGRP(87−132) by satisfying experimental structural restraints derived from structural templates of homologous proteins and from our mutagenesis data. In both calculated receptor−ligand complexes, the Arg-Phe-Phe motif of the antagonist interacts with negatively charged and aromatic residues of the receptor. However, they do so in a slightly different manner because of a small rotation of ASIP and its shift toward TMH2 and TMH7 relative to the position of ASIP and AGRP within the hMC4R-binding pocket. This shift might be caused by the presence of bulky residues in MC1R. The detailed structural information on ligand−receptor complexes obtained in our studies may assist future attempts to optimize the selectivity, potency, and efficacy of recently proposed non-peptide MC4R agonists and antagonists (56−58) and the rational design and development of other MC3R/4R drugs.

ACKNOWLEDGMENT

We are grateful to Andrei Lomize for the provided software, assistance in the calculations, and valuable discussions and to Carrie Haskell-Luevano and Nigel Richards for the coordinates of their recently described model of the MC4R−AGRP complex (*24*).

REFERENCES

1. Gantz, I., and Fong, T. M. (2003) The melanocortin system, *Am. J. Physiol. Endocrinol. Metab. 284*, E468−E474.
2. Mountjoy, K. G., Kong, P. L., Taylor, J. A., Willard, D. H., and Wilkison, W. O. (2001) Melanocortin receptor-mediated mobilization of intracellular free calcium in HEK293 cells, *Physiol. Genomics 5*, 11−19.
3. Dinulescu, D. M., and Cone, R. D. (2000) Agouti and agouti-related protein: Analogies and contrasts, *J. Biol. Chem. 275*, 6695−6698.
4. MacNeil, D. J., Howard, A. D., Guan, X., Fong, T. M., Nargund, R. P., Bednarek, M. A., Goulet, M. T., Weinberg, D. H., Strack, A. M., Marsh, D. J., Chen, H. Y., Shen, C. P., Chen, A. S., Rosenblum, C. I., MacNeil, T., Tota, M., MacIntyre, E. D., and van der Ploeg, L. H. (2002) The role of melanocortins in body weight regulation: Opportunities for the treatment of obesity, *Eur. J. Pharmacol. 440*, 141−157.
5. Ollmann, M. M., Wilson, B. D., Yang, Y. K., Kerns, J. A., Chen, Y., Gantz, I., and Barsh, G. S. (1997) Antagonism of central melanocortin receptors *in vitro* and *in vivo* by agouti-related protein, *Science 278*, 135−138.
6. Yang, Y. K., Thompson, D. A., Dickinson, C. J., Wilken, J., Barsh, G. S., Kent, S. B., and Gantz, I. (1999) Characterization of agouti-related protein binding to melanocortin receptors, *Mol. Endocrinol. 13*, 148−155.
7. Quillan, J. M., Sadee, W., Wei, E. T., Jimenez, C., Ji, L., and Chang, J. K. (1998) A synthetic human agouti-related protein-(83−132)-NH2 fragment is a potent inhibitor of melanocortin receptor function, *FEBS Lett. 428*, 59−62.
8. Jackson, P. J., McNulty, J. C., Yang, Y. K., Thompson, D. A., Chai, B., Gantz, I., Barsh, G. S., and Millhauser, G. L. (2002) Design, pharmacology, and NMR structure of a minimized cystine knot with agouti-related protein activity, *Biochemistry 41*, 7565−7572.
9. Adan, R. A., and Kas, M. J. (2003) Inverse agonism gains weight, *Trends Pharmacol. Sci. 24*, 315−321.
10. Haskell-Luevano, C., and Monck, E. K. (2001) Agouti-related protein functions as an inverse agonist at a constitutively active brain melanocortin-4 receptor, *Regul. Pept. 99*, 1−7.
11. Chai, B. X., Neubig, R. R., Millhauser, G. L., Thompson, D. A., Jackson, P. J., Barsh, G. S., Dickinson, C. J., Li, J. Y., Lai, Y. M., and Gantz, I. (2003) Inverse agonist activity of agouti and agouti-related protein, *Peptides 24*, 603−609.
12. Nijenhuis, W. A., Oosterom, J., and Adan, R. A. (2001) AgRP-(83−132) acts as an inverse agonist on the human-melanocortin-4 receptor, *Mol. Endocrinol. 15*, 164−171.
13. Siegrist, W., Drozdz, R., Cotti, R., Willard, D. H., Wilkison, W. O., and Eberle, A. N. (1997) Interactions of α-melanotropin and agouti on B16 melanoma cells: Evidence for inverse agonism of agouti, *J. Recept. Signal Transduction Res. 17*, 75−98.
14. Tota, M. R., Smith, T. S., Mao, C., MacNeil, T., Mosley, R. T., van der Ploeg, L. H., and Fong, T. M. (1999) Molecular interaction of Agouti protein and Agouti-related protein with human melanocortin receptors, *Biochemistry 38*, 897−904.
15. Yang, Y., Chen, M., Lai, Y., Gantz, I., Yagmurlu, A., Georgeson, K. E., and Harmon, C. M. (2003) Molecular determination of agouti-related protein binding to human melanocortin-4 receptor, *Mol. Pharmacol. 64*, 94−103.
16. Haskell-Luevano, C., Monck, E. K., Wan, Y. P., and Schentrup, A. M. (2000) The agouti-related protein decapeptide (Yc-[CRFFNAFC]Y) possesses agonist activity at the murine melanocortin-1 receptor, *Peptides 21*, 683−689.
17. Yang, Y. K., Fong, T. M., Dickinson, C. J., Mao, C., Li, J. Y., Tota, M. R., Mosley, R., van der Ploeg, L. H., and Gantz, I. (2000) Molecular determinants of ligand binding to the human melanocortin-4 receptor, *Biochemistry 39*, 14900−14911.
18. McNulty, J. C., Thompson, D. A., Bolin, K. A., Wilken, J., Barsh, G. S., and Millhauser, G. L. (2001) High-resolution NMR structure of the chemically synthesized melanocortin receptor binding domain AGRP(87−132) of the agouti-related protein, *Biochemistry 40*, 15520−15527.
19. Fletcher, J. I., Chapman, B. E., Mackay, J. P., Howden, M. E., and King, G. F. (1997) The structure of versutoxin (δ-atracotoxin-Hv1) provides insights into the binding of site 3 neurotoxins to the voltage-gated sodium channel, *Structure 5*, 1525−1535.
20. Joseph, C. G., Bauzo, R. M., Xiang, Z., Shaw, A. M., Millard, W. J., and Haskell-Luevano, C. (2003) Elongation studies of the human agouti-related protein (AGRP) core decapeptide (Yc-[CRFFNAFC]Y) results in antagonism at the mouse melanocortin-3 receptor, *Peptides 24*, 263−270.
21. Millhauser, G. L., McNulty, J. C., Jackson, P. J., Thompson, D. A., Barsh, G. S., and Gantz, I. (2003) Loops and links: Structural insights into the remarkable function of the agouti-related protein, *Ann. N.Y. Acad. Sci. 994*, 27−35.
22. Yang, Y. K., Dickinson, C. J., Zeng, Q., Li, J. Y., Thompson, D. A., and Gantz, I. (1999) Contribution of melanocortin receptor exoloops to Agouti-related protein binding, *J. Biol. Chem. 274*, 14100−14106.
23. Haskell-Luevano, C., Cone, R. D., Monck, E. K., and Wan, Y. P. (2001) Structure activity studies of the melanocortin-4 receptor by *in vitro* mutagenesis: Identification of agouti-related protein (AGRP), melanocortin agonist, and synthetic peptide antagonist interaction determinants, *Biochemistry 40*, 6164−6179.
24. Wilczynski, A., Wang, X. S., Joseph, C. G., Xiang, Z., Bauzo, R. M., Scott, J. W., Sorensen, N. B., Shaw, A. M., Millard, W. J., Richards, N. G., and Haskell-Luevano, C. (2004) Identification of putative agouti-related protein(87−132)−melanocortin-4 receptor interactions by homology molecular modeling and validation using chimeric peptide ligands, *J. Med. Chem. 47*, 2194−2207.
25. Palczewski, K., Kumasaka, T., Hori, T., Behnke, C. A., Motoshima, H., Fox, B. A., Le Trong, I., Teller, D. C., Okada, T., Stenkamp, R. E., Yamamoto, M., and Miyano, M. (2000) Crystal

structure of rhodopsin: A G protein-coupled receptor, *Science 289*, 739−745.
26. Li, J., Edwards, P. C., Burghammer, M., Villa, C., and Schertler, G. F. (2004) Structure of bovine rhodopsin in a trigonal crystal form, *J. Mol. Biol. 343*, 1409−1438.
27. Yang, Y., Dickinson, C., Haskell-Luevano, C., and Gantz, I. (1997) Molecular basis for the interaction of [Nle^4,D-Phe^7]melanocyte stimulating hormone with the human melanocortin-1 receptor, *J. Biol. Chem. 272*, 23000−23010.
28. Yang, Y. K., Dickinson, C., Lai, Y. M., Li, J. Y., and Gantz, I. (2001) Functional properties of an agouti signaling protein variant and characteristics of its cognate radioligand, *Am. J. Physiol. Regul. Integr. Comp. Physiol. 281*, R1877−R1886.
29. DeBlasi, A., O'Reilly, K., and Motulsky, H. J. (1989) Calculating receptor number from binding experiments using same compound as radioligand and competitor, *Trends Pharmacol. Sci. 10*, 227−229.
30. Eswar, N., John, B., Mirkovic, N., Fiser, A., Ilyin, V. A., Pieper, U., Stuart, A. C., Marti-Renom, M. A., Madhusudhan, M. S., Yerkovich, B., and Sali, A. (2003) Tools for comparative protein structure modeling and analysis, *Nucleic Acids Res. 31*, 3375−3380.
31. Sali, A., and Blundell, T. L. (1993) Comparative protein modelling by satisfaction of spatial restraints, *J. Mol. Biol. 234*, 779−815.
32. Vriend, G. (1990) What if: A molecular modeling and drug design program, *J. Mol. Graphics 8*, 52 and *6*, 29.
33. Sanchez, R., Pieper, U., Mirkovic, N., de Bakker, P. I., Wittenstein, E., and Sali, A. (2000) MODBASE, a database of annotated comparative protein structure models, *Nucleic Acids Res. 28*, 250−253.
34. Pogozheva, I. D., Lomize, A. L., and Mosberg, H. I. (1997) The transmembrane 7-α-bundle of rhodopsin: Distance geometry calculations with hydrogen bonding constraints, *Biophys. J. 72*, 1963−1985.
35. Pogozheva, I. D., Lomize, A. L., and Mosberg, H. I. (1998) Opioid receptor three-dimensional structures from distance geometry calculations with hydrogen bonding constraints, *Biophys. J. 75*, 612−634.
36. Fowler, C. B., Pogozheva, I. D., LeVine, H., III, and Mosberg, H. I. (2004) Refinement of a homology model of the μ-opioid receptor using distance constraints from intrinsic and engineered zinc-binding sites, *Biochemistry 43*, 8700−8710.
37. Guntert, P., and Wuthrich, K. (1991) Improved efficiency of protein structure calculations from NMR data using the program DIANA with redundant dihedral angle constraints, *J. Biomol. NMR 1*, 447−456.
38. Schioth, H. B., Petersson, S., Muceniece, R., Szardenings, M., and Wikberg, J. E. (1997) Deletions of the N-terminal regions of the human melanocortin receptors, *FEBS Lett. 410*, 223−228.
39. Tarnow, P., Schoneberg, T., Krude, H., Gruters, A., and Biebermann, H. (2003) Mutationally induced disulfide bond formation within the third extracellular loop causes melanocortin 4 receptor inactivation in patients with obesity, *J. Biol. Chem. 278*, 48666−48673.
40. Frandberg, P. A., Doufexis, M., Kapas, S., and Chhajlani, V. (2001) Cysteine residues are involved in structure and function of melanocortin 1 receptor: Substitution of a cysteine residue in transmembrane segment two converts an agonist to antagonist, *Biochem. Biophys. Res. Commun. 281*, 851−857.
41. Lagerstrom, M. C., Klovins, J., Fredriksson, R., Fridmanis, D., Haitina, T., Ling, M. K., Berglund, M. M., and Schioth, H. B. (2003) High affinity agonistic metal ion binding sites within the melanocortin 4 receptor illustrate conformational change of transmembrane region 3, *J. Biol. Chem. 278*, 51521−51526.
42. Nickolls, S. A., Cismowski, M. I., Wang, X., Wolff, M., Conlon, P. J., and Maki, R. A. (2003) Molecular determinants of melanocortin 4 receptor ligand binding and MC4/MC3 receptor selectivity, *Pharmacol. Exp. Ther. 304*, 1217−1227.
43. Hwa, J., Reeves, P. J., Klein-Seetharaman, J., Davidson, F., and Khorana, H. G. (1999) Structure and function in rhodopsin: Further elucidation of the role of the intradiscal cysteines, Cys-110, -185, and -187, in rhodopsin folding and function, *Proc. Natl. Acad. Sci. U.S.A. 96*, 1932−1935.
44. Holst, B., Elling, C. E., and Schwartz, T. W. (2002) Metal ion-mediated agonism and agonist enhancement in melanocortin MC1 and MC4 receptors, *J. Biol. Chem. 277*, 47662−47670.
45. Holst, B., and Schwartz, T. W. (2003) Molecular mechanism of agonism and inverse agonism in the melanocortin receptors: Zn^{2+} as a structural and functional probe, *Ann. N.Y. Acad. Sci. 994*, 1−11.
46. Farooqi, I. S., Keogh, J. M., Yeo, G. S., Lank, E. J., Cheetham, T., and O'Rahilly, S. (2003) Clinical spectrum of obesity and mutations in the melanocortin 4 receptor gene, *N. Engl. J. Med. 348*, 1085−1095.
47. Riek, R. P., Rigoutsos, I., Novotny, J., and Graham, R. M. (2001) Non-α-helical elements modulate polytopic membrane protein architecture, *J. Mol. Biol. 306*, 349−362.
48. Keefe, L. J., Sondek, J., Shortle, D., and Lattman, E. E. (1993) The α aneurism: A structural motif revealed in an insertion mutant of staphylococcal nuclease, *Proc. Natl. Acad. Sci. U.S.A. 90*, 3275−3279.
49. John, B., and Sali, A. (2003) Comparative protein structure modeling by iterative alignment, model building, and model assessment, *Nucleic Acids Res. 31*, 3982−3992.
50. Tao, Y. X., and Segaloff, D. L. (2003) Functional characterization of melanocortin-4 receptor mutations associated with childhood obesity, *Endocrinology 144*, 4544−4551.
51. Yeo, G. S., Lank, E. J., Farooqi, I. S., Keogh, J., Challis, B. G., and O'Rahilly, S. (2003) Mutations in the human melanocortin-4 receptor gene associated with severe familial obesity disrupts receptor function through multiple molecular mechanisms, *Hum. Mol. Genet. 12*, 561−574.
52. Hwa, J., Klein-Seetharaman, J., and Khorana, H. G. (2001) Structure and function in rhodopsin: Mass spectrometric identification of the abnormal intradiscal disulfide bond in misfolded retinitis pigmentosa mutants, *Proc. Natl. Acad. Sci. U.S.A. 98*, 4872−4876.
53. Frandberg, P. A., Xu, X., and Chhajlani, V. (1997) Glutamine235 and arginine272 in human melanocortin 5 receptor determines its low affinity to MSH, *Biochem. Biophys. Res. Commun. 236*, 489−492.
54. Yang, X., Wang, Z., Dong, W., Ling, L., Yang, H., and Chen, R. (2003) Modeling and docking of the three-dimensional structure of the human melanocortin 4 receptor, *J. Protein Chem. 22*, 335−344.
55. Horn, F., Vriend, G., and Cohen, F. E. (2001) Collecting and harvesting biological data: The GPCRDB and NucleaRDB information systems, *Nucleic Acids Res. 29*, 346−349.
56. Pan, K., Scott, M. K., Lee, D. H., Fitzpatrick, L. J., Crooke, J. J., Rivero, R. A., Rosenthal, D. I., Vaidya, A. H., Zhao, B., and Reitz, A. B. (2003) 2,3-Diaryl-5-anilino[1,2,4]thiadiazoles as melanocortin MC4 receptor agonists and their effects on feeding behavior in rats, *Bioorg. Med. Chem. 11*, 185−192.
57. Arasasingham, P. N., Fotsch, C., Ouyang, X., Norman, M. H., Kelly, M. G., Stark, K. L., Karbon, B., Hale, C., Baumgartner, J. W., Zambrano, M., Cheetham, J., and Tamayo, N. A. (2003) Structure−activity relationship of (1-aryl-2-piperazinylethyl)-piperazines: Antagonists for the AGRP/melanocortin receptor binding, *J. Med. Chem. 46*, 9−11.
58. Thompson, D. A., Chai, B. X., Rood, H. L., Siani, M. A., Douglas, N. R., Gantz, I., and Millhauser, G. L. (2003) Peptoid mimics of agouti related protein, *Bioorg. Med. Chem. Lett. 13*, 1409−1413.
59. Ballesteros, J. A., and Weinstein, H. (1995) Integrated methods for the construction of three-dimensional models and computational probing of structure−function relations in G-protein coupled receptors, *Methods Neurosci. 25*, 366−428.

BI0478704